Edge states of bilayer graphene in the quantum Hall regime

V. Mazo and E. Shimshoni
Department of Physics, Bar-Ilan University, Ramat Gan 52900, Israel

H. A. Fertig
Department of Physics, Indiana University, Bloomington, Indiana 47405, USA
(Received 30 December 2010; revised manuscript received 18 April 2011; published 5 July 2011)

We study the low-energy edge states of bilayer graphene in a strong perpendicular magnetic field. Several possible simple boundary geometries related to zigzag edges are considered. Tight-binding calculations reveal three types of edge-state behaviors: weakly, strongly, and nondispersive edge states. These three behaviors may all be understood within a continuum model, and related by nonlinear transformations to the spectra of quantum Hall edge states in a conventional two-dimensional electron system. In all cases, the edge states closest to zero energy include a holelike edge state of one valley and a particlelike state of the other on the same edge, which may or may not cross, depending on the boundary condition. Edge states with the same spin generically have anticrossings that complicate the spectra, but which may be understood within degenerate perturbation theory. The results demonstrate that the number of edge states crossing the Fermi level in clean, undoped bilayer graphene depends *both* on boundary conditions and the energies of the bulk states.

DOI: 10.1103/PhysRevB.84.045405 PACS number(s): 73.22.Pr, 73.43.−f, 71.10.Pm

I. INTRODUCTION AND PRINCIPAL RESULTS

The integer quantized Hall effect is a generic behavior of two-dimensional electron systems in a strong perpendicular magnetic field.[1–4] The primary manifestation of the effect is a precise quantization of the Hall conductance σ_{xy} to integer multiples of e^2/h, with the coefficient determined by the electron density. That this system can carry current at all is in some ways surprising, because the spectrum of the bulk system takes the form of Landau levels, highly degenerate states at discrete energy values, with gaps separating these isolated sets of states. With chemical potential placed in any of these gaps, one naively expects the system to be insulating. A basic explanation for the existence of Hall currents in clean systems involves edge states:[5] the energies of the Landau level states disperse as their guiding center quantum numbers[2] X approach the physical edge of the sample, and are thus current-carrying in a particular direction for a given edge. A difference in the occupation of states at opposite edges of the sample leads to a net current, with a voltage difference perpendicular to that current,[6] such that their ratio yields a Hall conductivity quantized at the number of distinct edge state branches that cross the Fermi level at a given edge.[5] When the chemical potential lies in an energy gap in the bulk of the system, the only low-energy excitations of the system are present at its edges. These dominate the low-energy physics of the system.

More recently, it has been recognized that the presence of gapless edge states in a system with a bulk energy gap is the defining characteristic of a more general class of systems, known as topological insulators.[7,8] Interestingly, in such systems, states with different quantum numbers at the same edge may cross the Fermi energy such that they carry current in opposing directions, so that there are both holelike and particlelike currents at the same edge. These states can be topologically protected from backscattering, and allow the transport of currents without dissipation. In addition, in such systems one may observe transport of quantities other than electric charge (e.g., spin) along their edges while carrying no electric current. The realization of such currents would be a major step in the exploitation of degrees of freedom beyond charge in electronic devices.[9,10]

One system known to possess this sort of behavior is graphene. Graphene is a two-dimensional honeycomb lattice of carbon atoms, which recently has become available in the laboratory.[11–13] Electronic states near the Fermi energy in this system largely reside in p_z orbitals of the carbon atoms, and when undoped, the low-energy continuum description of the electron states is best given in terms of the Dirac equation.[14,15] With an appropriate spin-orbit coupling term, it was shown that single-layer graphene could become a topological insulator even in the absence of a magnetic field.[16] However, subsequent estimates of the strength of this spin-orbit coupling in real graphene suggested that the effect would be very difficult to observe.[17–19]

Crossing of edge states with different quantum numbers can nevertheless be realized in single-layer graphene in the quantum Hall regime.[20,21] This is due to its unique Landau level spectrum, which has both positive and negative energy states (and is particle-hole symmetric), with the former supporting upwardly dispersing edge states and the latter downward dispersing edge states. In the absence of interactions and Zeeman coupling, there are four Landau levels precisely at zero energy in the bulk, with each spin state supporting a particlelike and a holelike edge state at each edge. When Zeeman coupling is included, the two spin states split so that one holelike state crosses one electronlike state at each edge. This allows for dissipationless spin transport at the edges.[21] The inclusion of electron-electron interactions transforms the crossing edge states into a magnetic domain wall with Luttinger liquid properties.[22] This structure may explain the presence of apparently metallic behavior for undoped graphene in magnetic fields of order $\sim$10 T,[23–25] which gives way to an insulating state in stronger fields.[26,27]

The rich physics associated with crossing edge states suggests that one may expect to find unusual behaviors in

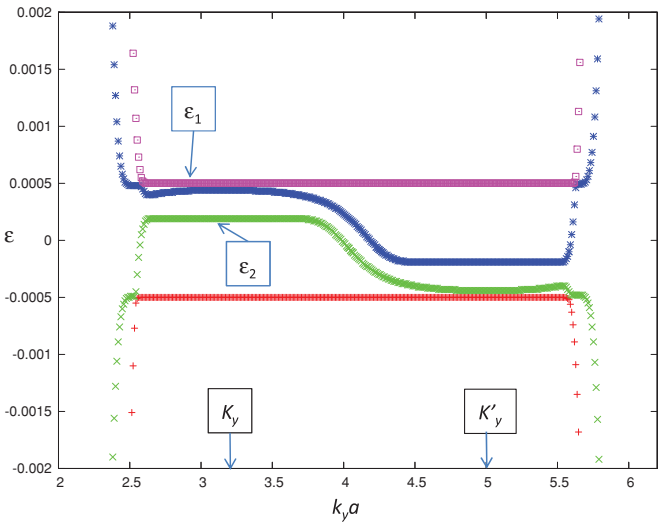

FIG. 1. (Color online) Energy bands of a Bernal-stacked graphene bilayer nanoribbon, $N = 240$ atoms across in each layer, each with zigzag edges. Perpendicular field is 100 T, interlayer bias $V = 0.001t$, and $\gamma_1 = 0.25t$, with t the in-plane hopping amplitude.

other systems that support both particle- and holelike edge states. In this context, bilayer graphene is a particularly interesting candidate to investigate. Even in the presence of interlayer coupling, bilayer graphene supports (in the absence of Zeeman coupling) eight zero-energy states.[28] Unlike the single-layer case, this degeneracy can be broken and controlled using an external, perpendicular electric field.[29] This raises the possibility of controlling the edge-state structure via a combination of this electric field and the Zeeman coupling (which may be manipulated using a parallel magnetic field). In what follows, we investigate the edge-state structure of a bilayer graphene ribbon using both tight-binding calculations and the Dirac equation, assuming appropriate boundary conditions for the latter. We focus on ribbons with zigzag edges,[30] as well as some simple extensions of this involving "bearded" edges[31] at a given edge.

Figure 1 illustrates a typical spectrum for the energy states of a graphene bilayer nanoribbon in a perpendicular magnetic field, as a function of k_y, the wave vector along the ribbon. One may see two regions supporting very flat bands in the vicinity of the $\hat{y}$ component of the vectors $\mathbf{K}$ and $\mathbf{K}'$, the locations of the Dirac points in the Brillouin zone of a graphene sheet. These results are consistent with those obtained in previous studies.[29,32] The bulk states for the valley on the left appear at energies $\varepsilon_1 = V/2$, where V is the potential energy difference between the layers due to a voltage bias, and, in the limit of small V,

$$\varepsilon_2 \approx \frac{V}{2}\,\frac{\gamma_1^2 - \omega_c^2}{\gamma_1^2 + \omega_c^2}\,. \tag{1}$$

Here γ_1 is the hopping amplitude between overlaid sites of the Bernal-stacked layers, $\omega_c = \sqrt{2}\hbar v_F/\ell$ in which $\ell = \sqrt{c\hbar/eB}$ is the magnetic length associated with the perpendicular magnetic field B, and v_F is the speed of electrons in the vicinity of a Dirac point in the absence of interlayer hopping. Analogous bulk energy states are present around K'_y at $\varepsilon'_1 = -\varepsilon_1$ and $\varepsilon'_2 = -\varepsilon_2$.

From the form of ε_1, it is clear that the wave functions corresponding to this band reside in a single sheet [see Eq. (4) below]. For the right edge, one finds no dispersion in this energy band, so that this edge state cannot contribute to the Hall conductivity of the system. Such *nondispersive* edge states are one type of behavior that is supported by the bilayer graphene edge, and are very analogous to those of the zeroth Landau level of a single graphene layer with a zigzag edge.[33]

At the same edge, ε_2 disperses downward, and we shall see that its dispersion has the approximate form

$$\varepsilon_2^{\text{edge}} \approx \frac{V}{2}\,\frac{\left[\gamma_1^2 - \omega_c^2 f(X)\right]}{\left[\gamma_1^2 + \omega_c^2 f(X)\right]}, \tag{2}$$

where $f(X)$, which may be determined variationally, grows monotonically from 1 when X is deep in the system bulk to large positive values when X is well over the system edge. This means that one expects the edge state to disperse *downward*, from the bulk value ε_2 to a value close to $-V/2$, as is apparent in Fig. 1. Because the range of energies available to these edge states is limited, they disperse relatively slowly, and represent a second type of edge state that is supported by the bilayer graphene system.

On the left edge of the system, there is an edge state that originates in the $\mathbf{K}'$ valley at $-\varepsilon_2$, and approaches $V/2$ as X moves well outside the bulk [in analogy with Eq. (2)]. Rather than becoming degenerate with ε_1, this begins to disperse downward as the edge is approached, so that ultimately there are both particlelike and holelike states dispersing from the vicinity of ε_1. This is analogous to the single-layer case,[33] for which a zigzag edge supports both particle-like and hole-like branches dispersing from the $n = 0$ Landau level. Note that these states disperse rapidly toward $\pm\infty$ as the wave-function centers move across the edge, representing a third type of behavior supported by this system, and is most similar to behaviors apparent in conventional quantum Hall systems.[5] We will see below that these states are most simply understood in terms of the $n = 0$ single-layer edge states, coupled together by γ_1, resulting in level repulsion and anticrossings.

This complicated structure suggests interesting possibilities for the low-energy edge states in bilayer graphene. For Fermi level precisely at zero energy ($\nu = 0$) and V exceeding the Zeeman splitting, one finds counterpropagating edge states for each spin, one from each valley, at a given edge: a right-moving $\mathbf{K}$ valley state (band ε_2) and a left-moving $\mathbf{K}'$ valley state (band ε'_2) reside on the left edge (see Fig. 1), and their symmetric counterparts reside on the right edge. This contrasts strongly with the $\nu = 0$ state of a conventional two-dimensional electron system, for which there are no edge states at all, and an insulator is formed for arbitrarily small disorder. In principle, the counterpropagating states will mix and localize due to disorder, but because they are well-separated in k_y, the localization length could be relatively long. Thus charge transport due to these edge states might be observable over short distance scales, in relatively clean samples. It is also possible that they could be observed in thermal transport.[34,35]

On the other hand, for large Zeeman splitting E_Z and small V, both electronlike states above $(V - E_Z)/2$ for spin-up states will cross the holelike states below $(E_Z - V)/2$ at zero

energy. In the absence of perturbations that can admix different spin states,[27] these channels will remain open so that $\nu = 0$ would become a quantized spin Hall state.[16]

Finally, it is interesting to note that if the ratio γ_1/ω_c can be tuned below 1, ε_2 would fall below 0, and no edge states would cross the Fermi level at all when $\nu = 0$ if the Zeeman coupling is sufficiently small. In principle, this can be accomplished with large magnetic fields, but would require values well above those currently available in the laboratory for the bare value of γ_1. It is possible, however, that the effective value of γ_1 could be decreased by an in-plane magnetic field. Presuming the energy ε_2 can be made to cross through zero energy for the undoped system, this leads to the possibility of driving a topological phase transition within the $\nu = 0$ state. The change in the edge-state structure for such a transition would be accompanied by a bulk change in the state, from a partially valley-polarized to an unpolarized state.

The remainder of this paper is organized as follows. In Sec. II, we describe our tight-binding results for the edge-state structure in more detail, and show how the results evolve from the single-layer results[33] as interlayer tunneling is turned on from zero. Section III discusses the continuum representation of these results. We conclude with a summary and some speculations in Sec. IV.

II. NUMERICAL RESULTS FOR THE TIGHT-BINDING MODEL

A. Zigzag edges

Our numerical calculations are based on a simple nearest-neighbor tight-binding model for graphene, with hopping amplitude t, which we take as our unit of energy in what follows. The basic unit for the bilayer crystal structure is illustrated in Fig. 2, in which there is an upper and lower layer whose bonding structure is indicated. In addition, there is a hopping matrix element γ_1 connecting sites lying above/below one another [red ($\tilde{A}$) and yellow (B) atoms in Fig. 2]. The graphene bilayer may also have longer-range interlayer hopping parameters γ_3 and γ_4, whose effect we assume to be negligible in the presence of a perpendicular magnetic field.[28] We consider the unit-cell structure, which has width a, to be infinitely repeated in the $\hat{y}$ direction, and to be repeated a finite number of times in the $\hat{x}$ direction. The resulting structure has zigzag edges in both layers on both sides of the ribbon.

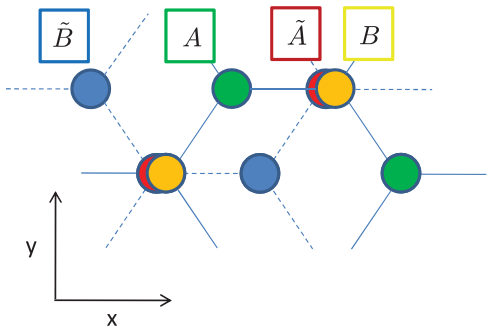

FIG. 2. (Color online) Unit cell for Bernal-stacked graphene bilayer nanoribbon, with zigzag edges. Dashed lines indicate bonds on the lower layer, solid lines are bonds on the upper layer.

Other edge constructions can be generated by removing atoms at the edge from the top or bottom layer. Removing an odd number of atoms from one of the layers in this way generates a "bearded" edge[31]; removing an even number returns the edge to a zigzag form. We explore two such constructions below. To implement the magnetic field, we introduce a vector potential into the hopping matrix element between neighboring atoms a and b in the standard way, $t \to t \exp\left[i\frac{e}{c}\int_a^b \mathbf{A}\cdot d\mathbf{r}\right]$, where $\mathbf{A}$ is the vector potential associated with the magnetic field, and we have taken $\hbar = 1$. Note that in order to avoid using excessively large numbers of atoms in a unit cell, we set the magnetic field to be rather large ($B = 100$ T), so that our ribbon is several magnetic lengths across. Although this is beyond what is typically attainable in the laboratory, our results should be qualitatively the same as for wider ribbons in lower magnetic fields.

Given the form of the tight-binding model, it is clear that there should be a continuous evolution of the spectra from that of decoupled layers ($\gamma_1 = 0$) to the form exhibited in Fig. 1 for physical values of γ_1 [estimated as 0.4 eV (Ref. 14)]. Figure 3 shows an example of this for a series of γ_1 values, from $\gamma_1 = 0.05\,t$ to $0.2\,t$. Note that guiding center coordinates for the single-particle states connected to the bulk states at $\mathbf{K}$ have the form $X = (k_y - K_y)\ell^2$, up to an overall constant. Where the bands begin to strongly diverge from their bulk energies as a function of k_y, the guiding center coordinate comes close to the physical edge of the system. This is easily confirmed by the form of the wave functions.

For the smallest value [Fig. 3(a)], it is clear that the basic structure of the spectrum involves particlelike and holelike edge states, each dispersing from bulk bands around $\varepsilon = \pm V/2$. The two states converging toward zero energy are admixed by γ_1, creating an anticrossing. Note the gap associated with this anticrossing is relatively large, because $\gamma_1 \gg V$. Thus one sees the spectrum is largely similar to that of two uncoupled layers at different constant potentials. For all the results shown in Fig. 3, when X is sufficiently inside the bulk that the effect of the edge is quite small, one may see that the two levels closest to zero always initially approach one another as X moves toward the edge. The two modes then anticross, and furthermore anticross with the levels closest to $\pm V/2$. Interestingly, the two modes at $\pm V/2$ persist to slightly larger values of k_y before diverging to large values of $|\varepsilon|$. Note that of these two modes, the positive energy one is an edge mode of the bulk band in the $\mathbf{K}$ valley at $\varepsilon = V/2$, while the negative one is the continuation of an edge state associated with a bulk band at $-V/2$ for the $\mathbf{K}'$ valley.

Edge states associated with the $\mathbf{K}$ valley for the other side of the ribbon behave relatively smoothly compared to the above, and are plainly visible in Fig. 1. This consists of a dispersionless edge state at $\varepsilon = V/2$ associated with the bulk band ε_1, and an edge state dispersing downward from ε_2 toward $-V/2$, where it continuously joins to the particlelike branch of the edge states (for $\gamma_1 \to 0$) associated with the bulk state at $-V/2$ of the $\mathbf{K}'$ valley. As we discuss in Sec. III, the behavior of these two states can be understood in a relatively straightforward manner from the continuum description of this system with appropriate boundary conditions.

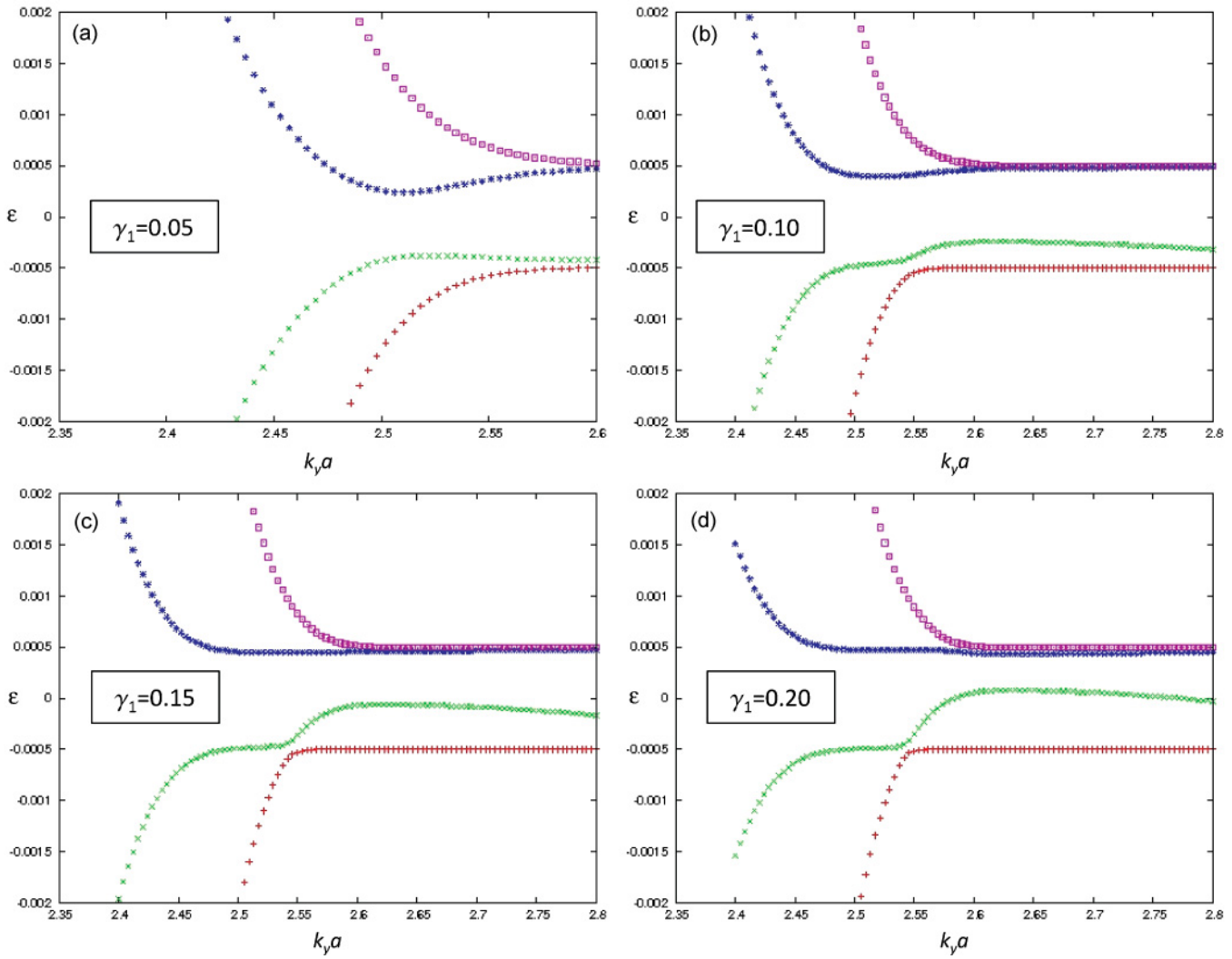

FIG. 3. (Color online) Detail of tight-binding energy bands of zigzag bilayer ribbon, near left edge of system, for state emerging from Landau levels of the K valley. The unit cell contains 480 atoms, perpendicular field is 100 T, and $V = 0.001$ (in units of t). Results illustrated for several values of γ_1.

B. Variants on the bilayer zigzag edge

We next discuss the edge-state spectra for two variants of the zigzag edge, known as the "bearded" edge.[31] This structure is created from a zigzag ribbon edge by removing the outermost atoms at the edge. The structure can also be created by adding single atoms to the outermost points of zigzag edge.

In the bilayer, structures involving bearded edges naturally emerge if one cuts all the bonds along a line in the zigzag direction. In addition to the zigzag geometry illustrated in Fig. 1, two other possibilities arise, as illustrated in the insets of Figs. 4 and 5. The edges in these two latter cases both involve a single zigzag edge in one layer and a bearded edge in the other. Unlike the ribbon with two zigzag edges, these ribbons present atoms on the *same* sublattice at both edges. The difference between the two zigzag-bearded edge ribbons is that in one case the atoms at an edge are uncoupled between layers, whereas in the other case the two outermost atoms form an interlayer dimer.

The spectrum of the former case is illustrated in the main panel of Fig. 4. Prominently visible are bands of constant energy precisely at $\pm V/2$. Such bands across the Brillouin zone are also visible when $\gamma_1 = 0$, the spectra of two single-layer ribbons at potentials $\pm V/2$, each with one bearded edge and one standard zigzag edge (see Fig. 6). In terms of a continuum model, this latter result has a simple interpretation: for the $\mathbf{K}'$ valley of the bottom $(-V/2)$ layer, the boundary condition may be taken to be vanishing of the A sublattice component on both edges, leading to dispersionless edge states on both sides. In this structure the dispersionless state of the left edge continues through the $\mathbf{K}$ valley. However, it has no simple interpretation in terms of $\mathbf{K}$ valley states within a continuum description. These states are very localized on the edge atoms of the bearded edge, and because their hybridization with the rest of the ribbon is extremely weak, and there is no hopping directly among them, the energy of the state is essentially pinned at $-V/2$.

For the $\mathbf{K}$ valley, the boundary condition in the same layer is a vanishing wave-function component on sublattice B, so that one finds the pair of dispersing particlelike and holelike edge states of the zeroth Landau level for a standard zigzag edge[33]

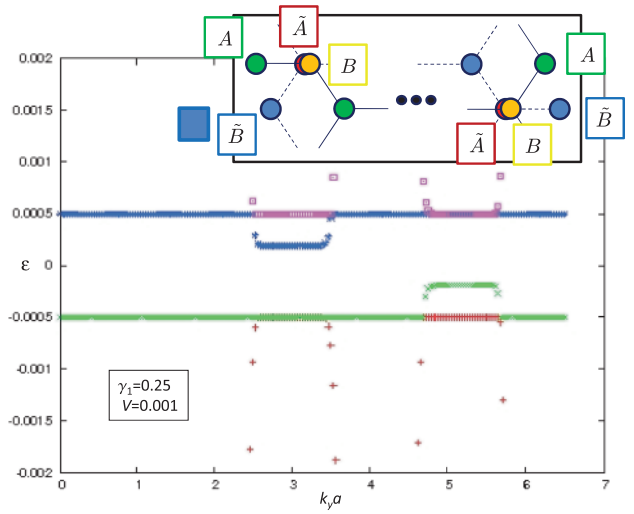

FIG. 4. (Color online) Energy states near zero for graphene ribbon with one layer bearded at each edge. The unit cell contains 474 atoms. Perpendicular field is 100 T, $V = 0.001$, and $\gamma_1 = 0.25$ (in units of t). Upper inset illustrates edges of the unit cell.

at *both* edges. Note the unusual situation that three bands are degenerate at $-V/2$ near the K_y point; the extra state is most naturally interpreted as a continuation of the $n = 0$ Landau level edge state from the $\mathbf{K}'$ valley.

This situation evolves in a simple way when γ_1 is increased from zero. For the K valley, the bulk mode at $\varepsilon_1 = V/2$ is localized on a single sublattice that is not directly affected by the boundary conditions, and so remains dispersionless at both edges. The other two $\mathbf{K}$ valley levels, which were degenerate at $-V/2$ for $\gamma_1 = 0$, evolve into a bulk mode at ε_2, which has particlelike edge states due to the boundary condition, and into an edge mode whose energy remains near $-V/2$

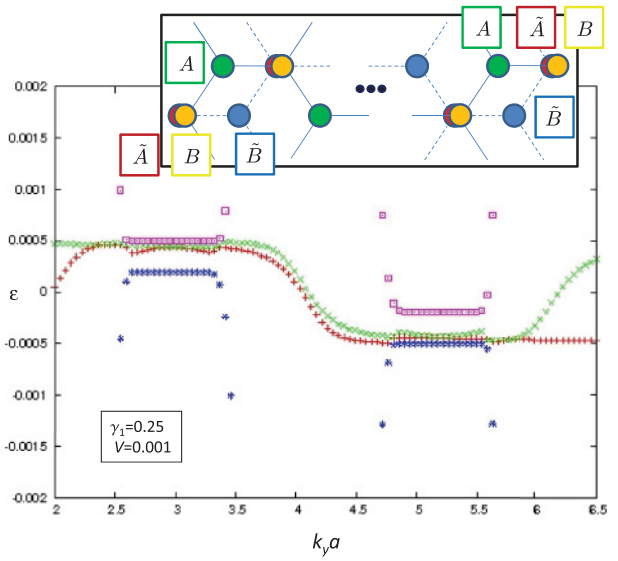

FIG. 5. (Color online) Energy states near zero for graphene ribbon with one layer bearded at each edge. Dimer atoms protrude at edges in this construction. The unit cell contains 478 atoms. Perpendicular field is 100, $V = 0.001$, and $\gamma_1 = 0.25$ (in units of t). Upper inset illustrates edges of the unit cell.

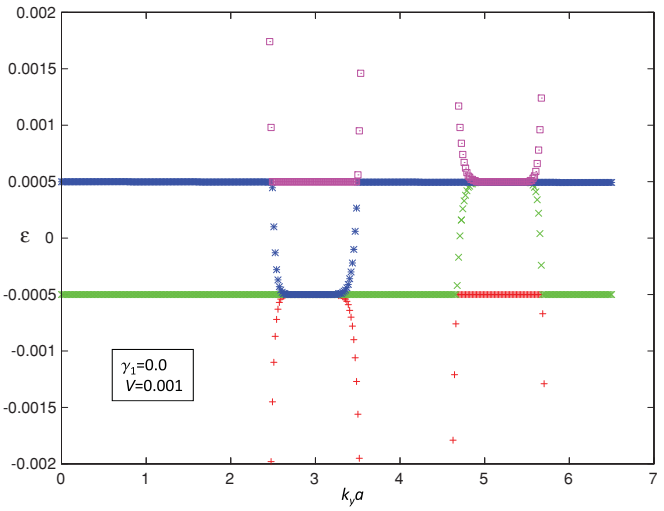

FIG. 6. (Color online) Energy states near zero for graphene ribbon with one layer bearded at each edge. Parameters are identical to those of Fig. 4, except $\gamma_1 = 0$.

for k_y sufficiently close to K_y, but develops a strong holelike dispersion away from the valley center. One also observes the edge state from the K′ valley at $-V/2$.

It is interesting to contrast this edge-state structure with what is apparent in Fig. 1. In addition to being considerably simpler, the edge-state structure of Fig. 4 has no slowly dispersing edge states, as is the case for the other edge constructions we consider. Moreover, there are no edge states of any kind crossing the Fermi level when it is at zero energy in this particular case. This demonstrates that in bilayer graphene, one may or may not have edge states crossing zero energy for the same bulk spectrum, depending on boundary conditions. In the former case, these are counterpropagating, so that no charge current is present at the edge in equilibrium, although these may transport energy.[34] That the presence or absence of low-energy edge excitations can depend on boundary conditions is somewhat unusual for a quantum Hall state, but is allowed because there are no strict quantum numbers distinguishing the counterpropagating states. When counterpropagating edge states carry *different* quantum numbers (e.g., spin), we expect their presence to be more robust.[22,27]

Finally, we consider the situation in which the outermost atoms at the edge are dimers, tunnel-coupled by γ_1. The corresponding spectrum is illustrated in Fig. 5. In this situation, there are no dispersionless states because the boundary conditions involve the sublattices on which the bulk states at $\varepsilon_{1,2}$ for the K valley (and $-\varepsilon_{1,2}$ for the $\mathbf{K}'$ valley) reside. Interestingly, we find two edge states that "thread" the gaps between the bulk states. Unlike the previous case, where each extra atom of a beard was connected to atoms only through a single bond, in this case these atoms are coupled to the zigzag edge of the opposing layer through γ_1. Thus it is not surprising that states localized on these sites would develop a dispersion, whereas in the previous case there was none. This situation is rather unique in supporting quasi-one dimensional states at the edge, which are not directly connected to any bulk state.

The behavior of the dispersive energy levels in each of the above-mentioned edge structures (Figs. 1, 4, and 5) can be

understood within a continuum theory with the appropriate boundary condition. This is described in detail in the next section.

III. CONTINUUM DESCRIPTION

We consider a Bernal-stacked bilayer graphene ribbon of finite width L in the $\hat{x}$ direction, where interlayer hopping is assumed to be only between the overlaid sites [red ($\tilde{A}$) and yellow (B) in Fig. 2] with an amplitude γ_1, and an interlayer voltage bias V is applied. Using a basis of 4-spinors $(\tilde{B},\tilde{A},B,A)$, where A, B ($\tilde{A}$, $\tilde{B}$) denote wavefunction components on sublattices A and B of the top (bottom) layer, and a gauge choice $\mathbf{A} = B_z x\hat{\mathbf{y}}$ for the vector potential, the Dirac Hamiltonian projected onto a given k_y in the vicinity of the valley $\mathbf{K}$ is given by the 4×4 matrix

$$\mathrm{H} = \begin{pmatrix} -V/2 & \omega_c a & 0 & 0 \\ \omega_c a^\dagger & -V/2 & \gamma_1 & 0 \\ 0 & \gamma_1 & V/2 & \omega_c a \\ 0 & 0 & \omega_c a^\dagger & V/2 \end{pmatrix} . \tag{3}$$

Here $a = \frac{1}{\sqrt{2}}[\partial_x + (x - X)]$ and $a^\dagger = \frac{1}{\sqrt{2}}[-\partial_x + (x - X)]$, where x and the guiding-center coordinate $X \equiv \ell(k_y - K_y)$ are in units of the magnetic length ℓ (i.e., dimensionless), and $\omega_c = \sqrt{2}\hbar v_F/\ell$. In the vicinity of the other valley ($\mathbf{K}'$ point), the same Hamiltonian (with $V \to -V$) applies in the basis of inverted 4-spinors $(A,B,\tilde{A},\tilde{B})$. As already discussed in Sec. I, for $V \ll \gamma_1,\omega_c$ the bulk solution for the energy spectrum of (3) includes two low-energy levels, $\varepsilon_1 = V/2$ and ε_2 [Eq. (1)]. The corresponding eigenfunctions are given by[32]

$$|\Psi_1\rangle = \begin{pmatrix} 0 \\ 0 \\ 0 \\ |0\rangle \end{pmatrix}, \quad |\Psi_2\rangle = \frac{1}{\mathcal{N}} \begin{pmatrix} 0 \\ |0\rangle \\ \frac{V\gamma_1}{\gamma_1^2+\omega_c^2}|0\rangle \\ -\frac{\gamma_1}{\omega_c}|1\rangle \end{pmatrix}, \tag{4}$$

in which $|n\rangle = \phi_n(x - X)$ are the harmonic-oscillator wave functions, and $\mathcal{N}$ is a normalization factor. The dispersion of ε_ν when X approaches the edge can be found by imposing the appropriate boundary condition at $x = \pm L/2$. Below we study separately four distinct boundary conditions, compatible with the tight-binding calculations of the previous section.

A. Right zigzag edge: $B(L/2) = \tilde{B}(L/2) = 0$

In a bilayer ribbon with zigzag edges including an integer multiple of unit cells, the boundary conditions at the right and left edges are fundamentally different. We first consider the right-hand edge ($x = L/2$), at which the wave function is forced to vanish on the B sublattice of both layers. We therefore look for solutions of the form $\mathbf{\Psi}_\nu^{\mathrm{edge}}(x) = (\tilde{B}(x),\tilde{A}(x),B(x),A(x))$, where $B(L/2) = \tilde{B}(L/2) = 0$. From Eq. (4) it is obvious that the bulk wave function $\mathbf{\Psi}_1$ already obeys this boundary condition, hence ε_1 is nondispersive in analogy with the monolayer case. In contrast, the component $B(x)$ of $\mathbf{\Psi}_2$ is nonvanishing; however, it is smaller than the components $A(x)$, $\tilde{A}(x)$ in the small V limit. This suggests that $\mathbf{\Psi}_2^{\mathrm{edge}}$ is given by a smooth deformation of $\mathbf{\Psi}_2$, which dictates a dispersion $\varepsilon_2^{\mathrm{edge}}(X)$ of the corresponding eigenvalue.

An exact analytic evaluation of $\varepsilon_2^{\mathrm{edge}}(X)$ is not possible. However, as we show next, an approximation based on either a variational calculation or a perturbation expansion in the interlayer hopping can explain the right-hand dispersion of ε_2 in Fig. 1.

We start with a variational approach, similar to the one adapted in Ref. 33 for a single-layer graphene. The variational ansatz on $\mathbf{\Psi}_2^{\mathrm{edge}}(x)$ is taken to be the simplest modification of the bulk function $\mathbf{\Psi}_2(x)$, which obeys the boundary condition. We therefore assume $\tilde{B}(x) = 0$, and apply the variational principle to the remaining three components, out of which only $B(x)$ is restricted by the vanishing boundary condition. Note that since the spectrum of the Dirac Hamiltonian is unbounded, the standard procedure of minimizing the energy expectation value $\varepsilon = \langle H\rangle$ is not applicable. However, it turns out to be possible to express it as a monotonic function of an "effective energy" functional with a well-defined minimum. To see this, we first impose the extremum condition $\delta\varepsilon/\delta A = \delta\varepsilon/\delta\tilde{A} = 0$, which yields

$$\tilde{A}(x) = \frac{\gamma_1}{(\varepsilon + V/2)} B(x) , \tag{5}$$

$$A(x) = \frac{1}{(\varepsilon - V/2)} \omega_c a^\dagger B(x) . \tag{6}$$

Evaluating $\langle H\rangle$ for this state, in the small V limit, produces an expression for ε as a functional of $B(x)$ only:

$$\varepsilon \approx \frac{V}{2} \frac{\left(\gamma_1^2 - \omega_c^2\langle aa^\dagger\rangle_B\right)}{\left(\gamma_1^2 + \omega_c^2\langle aa^\dagger\rangle_B\right)} , \tag{7}$$

where

$$\langle aa^\dagger\rangle_B \equiv \frac{\int dx B^*(x) aa^\dagger B(x)}{\int dx |B(x)|^2} = 1 + \langle a^\dagger a\rangle_B . \tag{8}$$

Quite interestingly, the expectation value $\langle a^\dagger a\rangle_B$ (implicitly dependent on X via the definition of a, $a^\dagger$) is equivalent (up to an additive constant) to the energy of a quantum Hall edge states in an ordinary two-dimensional (2D) electron gas. In particular, it is identical to the functional associated with the *square* of the energy of edge states in single-layer graphene,[33] and can be minimized using a standard variational ansatz for $B(x)$. Notice that minimizing $\langle a^\dagger a\rangle_B$ with respect to B also minimizes ε^2 in Eq. (7), giving estimates for the states closest to zero energy. The dispersion curve $f(X) = 1 + \min\{\langle a^\dagger a\rangle_B\}$ has a known qualitative behavior as a function of X: in the bulk, $B(x) = |0\rangle$, hence $f(X) = 1$; as X approaches the boundary, $f(X)$ increases monotonically and acquires large positive values when X is well beyond the edge. When substituted in Eq. (8), this yields the dispersive energy band

$$\varepsilon_2^{\mathrm{edge}}(X) = \frac{V}{2} \frac{\left[\gamma_1^2 - \omega_c^2 f(X)\right]}{\left[\gamma_1^2 + \omega_c^2 f(X)\right]}, \tag{9}$$

which decreases monotonically with X from the bulk value ε_2 to the saturated value $\varepsilon_2^{\mathrm{edge}}(X) \to -V/2$ as $f(X) \to \infty$.

An alternative approach to the derivation of the above dispersion law involves a perturbative expansion in γ_1. This approach turns out to be useful to develop insight about the prominent qualitative features of the spectrum for more complicated boundary conditions as well, even in the regime

where it is not strictly justified to assume γ_1 small. To this end, we define

$$\mathrm{H}' = \begin{pmatrix} 0 & 0 & 0 & 0 \\ 0 & 0 & \gamma_1 & 0 \\ 0 & \gamma_1 & 0 & 0 \\ 0 & 0 & 0 & 0 \end{pmatrix} \tag{10}$$

as a perturbation on $\mathrm{H}_0 \equiv \mathrm{H}_{\gamma_1=0}$ describing the uncoupled layers. The eigenstates of H_0 are single-layer Landau level (LL) states. Focusing first on bulk states, the zero LL states and corresponding energies (split by the interlayer bias V) are given by

$$\left|\Psi_1^{(0)}\right\rangle = |\Phi_0\rangle \equiv \begin{pmatrix} 0 \\ 0 \\ 0 \\ |0\rangle \end{pmatrix}, \quad \varepsilon_1^{(0)} = \frac{V}{2}, \tag{11}$$

$$\left|\Psi_2^{(0)}\right\rangle = |\tilde{\Phi}_0\rangle \equiv \begin{pmatrix} 0 \\ |0\rangle \\ 0 \\ 0 \end{pmatrix}, \quad \varepsilon_2^{(0)} = -\frac{V}{2}\,. \tag{12}$$

Since $\mathrm{H}'|\Psi_1^{(0)}\rangle = 0$, the perturbation does not couple the top-layer state [Eq. (11)] to higher LL's, so that $|\Psi_1^{(0)}\rangle = |\Psi_1\rangle$ [Eq. (4)] and $\varepsilon_1^{(0)}$ remains fixed at $\varepsilon_1 = V/2$ for arbitrarily large γ_1. In contrast, H' couples the bottom-layer state [Eq. (12)] to the $n = \pm 1$ LL states in the top layer,

$$|\Phi_{\pm 1}\rangle = \frac{1}{\sqrt{2}} \begin{pmatrix} 0 \\ 0 \\ |0\rangle \\ \pm|1\rangle \end{pmatrix}, \quad \varepsilon_{\pm 1} = \frac{V}{2} \pm \omega_c\,. \tag{13}$$

To second order in perturbation theory (and leading order in V/ω_c), the resulting correction to ε_2 is

$$\varepsilon_2^{(2)} = \sum_{n=\pm 1} \frac{|\langle \Phi_n | H_1 | \Phi_0 \rangle|^2}{\varepsilon_2^{(0)} - \varepsilon_n} \approx \frac{\gamma_1^2 V}{\omega_c^2}\,. \tag{14}$$

To leading order in γ_1/ω_c, the resulting $\varepsilon_2 = \varepsilon_2^{(0)} + \varepsilon_2^{(2)}$ coincides with Eq. (1).

We next consider edge states where X approaches the right edge boundary $L/2$. Since both $|\Phi_0\rangle$ and $|\tilde{\Phi}_0\rangle$ [Eqs. (11) and (12)] have vanishing components on the B sublattice, the boundary condition is obeyed and $\varepsilon_1^{(0)}$, $\varepsilon_2^{(0)}$ do not disperse. However, higher LL states are modified and consequently so is the energy eigenvalue ε_2 at finite γ_1. For $\gamma_1 = 0$, the wave functions and energies (13) become

$$\left|\Phi_{\pm 1}^R\right\rangle = \frac{1}{\mathcal{N}_R} \begin{pmatrix} 0 \\ 0 \\ |0_R\rangle \\ \pm\frac{1}{\sqrt{1+\lambda(X)}}|1_R\rangle \end{pmatrix}, \qquad \varepsilon_{\pm 1}^R = \frac{V}{2} \pm \sqrt{1+\lambda(X)}\,\omega_c, \tag{15}$$

where $|0_R\rangle|_{x=L/2} = 0$ so that $a^\dagger a|0_R\rangle = \lambda(X)|0_R\rangle$ with $\lambda(X) > 0$ the dispersion curve of a conventional lowest LL edge state, $|1_R\rangle \equiv a^\dagger|0_R\rangle$, and $\mathcal{N}_R$ is a normalization factor. Neglecting the contribution of higher LL, we obtain the second-order correction to ε_2,

$$\varepsilon_2^{R(2)}(X) \approx \frac{2\gamma_1^2 V}{\mathcal{N}_R^2} \frac{|\langle 0_R|0\rangle|^2}{\omega_c^2[1+\lambda(X)]}\,. \tag{16}$$

Note that Eq. (16) is similar to (14), with the expansion parameter γ_1/ω_c replaced by the X-dependent parameter $\gamma_1/\tilde{\omega}_c(X)$, where

$$\tilde{\omega}_c(X) \equiv \frac{\mathcal{N}_R \omega_c \sqrt{1+\lambda(X)}}{\sqrt{2}|\langle 0_R|0\rangle|}\,. \tag{17}$$

When X is pushed farther toward the edge, $\tilde{\omega}_c(X)$ is *monotonically increasing* due to a combination of the increase of $\lambda(X)$ in the numerator and the suppression of the overlap $|\langle 0_R|0\rangle|$ in the denominator. For X far beyond the physical edge, $\tilde{\omega}_c(X) \to \infty$. Hence, even in the physically relevant case where $\gamma_1/\omega_c > 1$, the effective perturbation expansion parameter becomes increasingly smaller, i.e., the coupling between layers effectively weakens. This behavior turns out to be valid for all types of boundary conditions. In the present case, we conclude that the dispersion curve $\varepsilon_2(X)$ is monotonically decreasing and asymptotically approaches $-V/2$ for $X \to \infty$, in agreement with the variational result Eq. (9).

B. Left zigzag edge: $A(-L/2) = \tilde{A}(-L/2) = 0$

The boundary condition on the left edge of the ribbon, $A(-L/2) = \tilde{A}(-L/2) = 0$, creates a much stronger disturbance for both electronic wave functions $|\Psi_1\rangle$, $|\Psi_2\rangle$ when X is close or to the left of $-L/2$, and changes their shape significantly. To analyze this case, we implement the perturbative approach introduced in the previous subsection. The uncoupled layers states $|\Phi_0\rangle$, $|\tilde{\Phi}_0\rangle$ and the corresponding energy levels [Eqs. (11) and (12)] are now split into two branches each:

$$|\Phi_{\pm 0}^L\rangle = \frac{1}{\mathcal{N}_0} \begin{pmatrix} 0 \\ 0 \\ \pm\frac{1}{\sqrt{\lambda(X)}}|\ell_L\rangle \\ |0_L\rangle \end{pmatrix}, \qquad \varepsilon_{\pm 0}^L(X) = \frac{V}{2} \pm \omega_c\sqrt{\lambda(X)}\,, \tag{18}$$

$$|\tilde{\Phi}_{\pm 0}^L\rangle = \frac{1}{\mathcal{N}_0} \begin{pmatrix} \pm\frac{1}{\sqrt{\lambda(X)}}|\ell_L\rangle \\ |0_L\rangle \\ 0 \\ 0 \end{pmatrix}, \qquad \tilde{\varepsilon}_{\pm 0}^L(X) = -\frac{V}{2} \pm \omega_c\sqrt{\lambda(X)}, \tag{19}$$

where $|0_L\rangle|_{x=-L/2} = 0$, $a^\dagger a|0_L\rangle = \lambda(X)|0_L\rangle$ [with $\lambda(X)$ the same as $\lambda(-X)$ of Eq. (15)], and $|\ell_L\rangle \equiv a|0_L\rangle$ a wave function strongly confined to the edge. Note that the holelike dispersive branch of the top-layer state $[\varepsilon_{-0}^L(X)]$ and the particlelike

branch of the bottom layer $[\tilde{\varepsilon}^L_{+0}(X)]$ cross at zero energy. When we next turn on a finite but small interlayer hopping γ_1, these two branches mix and a gap will open up, yielding an avoided crossing as observed in Fig. 3(a). For larger γ_1, each of the mixing branches separately will get modified and the band structure becomes more complicated. To leading order in perturbation theory, we consider the corrections due to mixing with higher LL states,

$$|\Phi^L_{\pm 1}\rangle = \frac{1}{\mathcal{N}_L}\begin{pmatrix} 0 \\ 0 \\ \pm\frac{1}{\sqrt{\lambda_1(X)}}|0'_L\rangle \\ |1'_L\rangle \end{pmatrix}, \qquad \varepsilon^L_{\pm 1} = \frac{V}{2} \pm \omega_c\sqrt{\lambda_1(X)}\,, \tag{20}$$

$$|\tilde{\Phi}^L_{\pm 1}\rangle = \frac{1}{\mathcal{N}_L}\begin{pmatrix} \pm\frac{1}{\sqrt{\lambda_1(X)}}|0'_L\rangle \\ |1'_L\rangle \\ 0 \\ 0 \end{pmatrix}, \qquad \tilde{\varepsilon}^L_{\pm 1} = -\frac{V}{2} \pm \omega_c\sqrt{\lambda_1(X)}, \tag{21}$$

where $|1'_L\rangle|_{x=-L/2} = 0$, $a^\dagger a|1'_L\rangle = \lambda_1(X)|1'_L\rangle$ with $\lambda_1(X) > 1$, and $|0'_L\rangle \equiv a|1'_L\rangle$. This yields the following approximations for the holelike and particlelike branches dispersing from the bulk energy levels ε_1, ε_2:

$$\varepsilon^L_{1,\pm}(X) \approx \frac{V}{2} \pm \omega_c\sqrt{\lambda(X)} - \frac{2\gamma_1^2|\langle 1'_L|\ell_L\rangle|^2[\pm\omega_c\sqrt{\lambda(X)}+V]}{\mathcal{N}_0^2\mathcal{N}_L^2\lambda(X)\{\omega_c^2[\lambda_1(X)-\lambda(X)] \mp 2V\omega_c\sqrt{\lambda(X)}\}}\,, \tag{22}$$

$$\varepsilon^L_{2,\pm}(X) \approx -\frac{V}{2} \pm \omega_c\sqrt{\lambda(X)} - \frac{2\gamma_1^2|\langle 0'_L|0_L\rangle|^2[\pm\omega_c\sqrt{\lambda(X)}-V]}{\mathcal{N}_0^2\mathcal{N}_L^2\lambda_1(X)\{\omega_c^2[\lambda_1(X)-\lambda(X)] \pm 2V\omega_c\sqrt{\lambda(X)}\}}\,. \tag{23}$$

In particular, the holelike branch $\varepsilon^L_{1,-}(X)$ and the particlelike branch $\varepsilon^L_{2,+}(X)$ develop a nontrivial (possibly nonmonotonic) dependence on X, which shifts their crossing away from zero energy. The gap opening at the avoided crossing point is given to leading order by degenerate perturbation theory as

$$\Delta_L(X) \approx \frac{\gamma_1}{\sqrt{\lambda(X)}\mathcal{N}_0^2}|\langle 0_L|\ell_L\rangle|\,. \tag{24}$$

As γ_1 becomes bigger, the second-order corrections in Eqs. (22) and (23) become increasingly dominant, and in particular the negative correction to $\varepsilon^L_{2,+}(X)$ can lead to the features observable in the spectrum depicted in Figs. 3(b)–3(d). However, it should be noted that (as in the previous case of boundary conditions, and for the same reason) the perturbative expansion systematically improves for the farthest edge states (corresponding to X very close to or beyond the left edge). The lowest-energy levels are then approximated by the particle-hole symmetric values $\pm[V/2 - \omega_c\sqrt{\lambda(X)}]$, consistent with Fig. 3.

C. Top-layer bearded edges $B(\pm L/2) = \tilde{A}(\pm L/2) = 0$

The next type of boundary condition corresponds to the edges depicted in Fig. 4. A special feature of this particular configuration is that an *identical* (vanishing) boundary condition is imposed on both wave-function components associated with the overlaid sites of the interlayer dimer, i.e., $B(\pm L/2) = \tilde{A}(\pm L/2) = 0$. Therefore, one can find a consistent solution to the Dirac equation $H|\Psi\rangle = \varepsilon|\Psi\rangle$ [where H is given by Eq. (3)] with $\tilde{A}(x)$, $B(x)$ being given by the same function (up to a constant prefactor).

To see this, we note that the Dirac equation can be cast as a set of four coupled equations:

$$\omega_c a\tilde{A} = (\varepsilon + V/2)\,\tilde{B}, \tag{25}$$

$$\omega_c a^\dagger\tilde{B} + \gamma_1 B = (\varepsilon + V/2)\,\tilde{A}, \tag{26}$$

$$\gamma_1\tilde{A} + \omega_c a A = (\varepsilon - V/2)\,B, \tag{27}$$

$$\omega_c a^\dagger B = (\varepsilon - V/2)\,A\,, \tag{28}$$

which can be combined to yield two coupled Schrödinger equations for the components $\tilde{A}$, B:

$$\left[\omega_c^2 a^\dagger a - (\varepsilon + V/2)^2\right]\tilde{A} = -\gamma_1(\varepsilon + V/2)B, \tag{29}$$

$$\left[\omega_c^2 a a^\dagger - (\varepsilon - V/2)^2\right]B = -\gamma_1(\varepsilon - V/2)\tilde{A}\,. \tag{30}$$

Clearly, there is a solution to Eqs. (29) and (30) of the form $\tilde{A} = c_A|0_e\rangle$, $B = c_B|0_e\rangle$ in which c_A, c_B are constants and $|0_e\rangle$ is an eigenstate of the operator $a^\dagger a$ satisfying the boundary condition. For X close to (or beyond) one of the edges $\pm L/2$, the function $|0_e\rangle$ satisfies the boundary condition $|0_e\rangle|_{x=\pm L/2} = 0$ and the Schrödinger equation

$$a^\dagger a|0_e\rangle = \lambda(X)|0_e\rangle\,; \tag{31}$$

here $\lambda(X)$ is the same dispersion curve introduced in the previous subsections, corresponding to the edge dispersion of a conventional LLL edge state. In fact, $|0_e\rangle$ coincides with $|0_R\rangle$ (Sec. III A) for $X > 0$, and $|0_L\rangle$ (Sec. III B) for $X < 0$. Substituting this ansatz in Eqs. (29) and (30), we get an eigenvalue equation for ε:

$$\frac{(\varepsilon - V/2)^2 - \omega_c^2[1+\lambda(X)]}{\gamma_1(\varepsilon - V/2)} = \frac{\gamma_1(\varepsilon + V/2)}{(\varepsilon + V/2)^2 - \omega_c^2\lambda(X)}. \tag{32}$$

For $V \ll \omega_c, \gamma_1$, the two lowest-energy solutions are

$$\varepsilon_{\pm}(X) \approx \frac{1}{\Gamma^2+1+2\lambda(X)}\left[-\frac{V}{2} \pm \sqrt{V^2\left(\frac{\Gamma^4}{4}-\lambda(X)[1+\lambda(X)]\right)+\omega_c^2\lambda(X)[1+\lambda(X)][\Gamma^2+1+2\lambda(X)]}\right], \tag{33}$$

where $\Gamma \equiv \gamma_1/\omega_c$.

We first note that the above calculation recovers the known bulk solution for $\lambda(X)=0$ and $|0_e\rangle = |0\rangle$. Indeed, Eq. (33) then yields $\varepsilon_+(X)=\varepsilon_2$ [Eq. (1)]. The apparent second solution $\varepsilon_- = -V/2$ does not correspond to a valid solution of the original Dirac equation: inserting $\tilde{A} = c_A|0\rangle$, $B = c_B|0\rangle$ in Eqs. (25) and (26) gives an ambiguous expression for the $\tilde{B}$ component. (This can be traced back to an assumption that $a^\dagger a|0_e\rangle \neq 0$, which is not the case when $|0_e\rangle$ is a bulk lowest Landau level state.) We therefore conclude that $\varepsilon_\pm(X)$ converges to a single bulk energy level ε_2, which (as noted earlier) has evolved from the zero Landau level bulk state of the uncoupled bottom layer. However, as soon as $\lambda(X)$ is finite, Eq. (33) dictates that the bulk state splits into two dispersive bands: $\varepsilon_+(X)$ is particlelike, and steeply deviates upward from ε_2 as X approaches the edge, i.e., with increasing $\lambda(X)$; $\varepsilon_-(X)$ is holelike, and steeply deviates downward from $-V/2$ as $\lambda(X)$ increases. This behavior is clearly seen in Fig. 4.

We finally comment that in addition to the above-mentioned dispersive energy bands, there exists a trivial solution to this boundary problem where $\tilde{A}=B=0$. Similarly to the case discussed in Sec. III A, this corresponds to the bulk wave function $|\Psi_1\rangle$ [see Eq. (4)], which is not affected by the boundary. As a consequence, there is no dispersion of the bulk energy level ε_1 and it is maintained fixed at $V/2$ for arbitrarily large $|X|$. The other valley ($\mathbf{K}'$ point) contributes another nondispersive state at energy $-V/2$, which corresponds to an eigenfunction $|\Psi_1'\rangle$ localized on the $\tilde{B}$ component only. Together with $\varepsilon_\pm(X)$, this explains the entire spectrum depicted in Fig. 4.

D. Bottom-layer bearded edges $A(\pm L/2) = \tilde{B}(\pm L/2) = 0$

The boundary condition corresponding to the edge structure depicted in Fig. 5 can be cast as $A(\pm L/2)=\tilde{B}(\pm L/2)=0$. Similar to the case discussed in Sec. III B, this imposes a strong perturbation on the low-energy states as both $|\mathbf{\Psi}_1\rangle$ and $|\mathbf{\Psi}_2\rangle$ [see Eq. (4)] have to be modified from their bulk form. We study this case using the perturbative approach introduced above. The unperturbed ($\gamma_1=0$) states satisfying the boundary conditions are given by edge states of the form $|\Phi^L_{\pm 0}\rangle$ [Eq. (18)] (with $|0_L\rangle, |\ell_L\rangle$ replaced by $|0_R\rangle, |\ell_R\rangle$ for right-edge states, i.e., $X>0$) and the bulk state $|\tilde{\Phi}_0\rangle$ [Eq. (12)]. Note that the lower-energy branch of the edge states, $\varepsilon^e_{-0}(X) = V/2 - \omega_c\sqrt{\lambda(X)}$ ($e=R,L$), is holelike and crosses the unperturbed bulk level $\varepsilon_2^{(0)} = -V/2$. Turning on the interlayer hopping γ_1 leads to a shift of the latter bulk level and its dispersion at the edge, and in addition to mixing of the crossing levels and an opening of a gap. As in Sec. III B, we first evaluate the dispersive energy bands $\varepsilon^e_{1,\pm}(X)$, $\varepsilon^e_{2,\pm}(X)$ resulting due to mixing with the higher LL $n=\pm 1$ to leading order in γ_1. The $n=\pm 1$ states of the uncoupled layers are given in this case by

$$|\Phi^e_{\pm 1}\rangle = \frac{1}{\mathcal{N}'_e}\begin{pmatrix} 0 \\ 0 \\ \pm\frac{1}{\sqrt{\lambda_1(X)}}|0'_e\rangle \\ |1'_e\rangle \end{pmatrix}, \qquad \varepsilon^e_{\pm 1} = \frac{V}{2} \pm \omega_c\sqrt{\lambda_1(X)}\,, \tag{34}$$

$$|\tilde{\Phi}^e_{\pm 1}\rangle = \frac{1}{\mathcal{N}_e}\begin{pmatrix} |0_e\rangle \\ \pm\frac{1}{\sqrt{1+\lambda(X)}}|1_e\rangle \\ 0 \\ 0 \end{pmatrix}, \qquad \tilde{\varepsilon}^e_{\pm 1} = -\frac{V}{2} \pm \omega_c\sqrt{1+\lambda(X)}, \tag{35}$$

where $|1'_e\rangle|_{x=\pm L/2}=0$, $|0'_e\rangle \equiv a|1'_e\rangle$, and $\lambda(X)$, $\lambda_1(X)$ are the same as in Sec. III B. The resulting perturbative expressions for the edge bands dispersing from ε_1, ε_2 are

$$\varepsilon^e_{1,\pm}(X) \approx \frac{V}{2} \pm \omega_c\sqrt{\lambda(X)} - \frac{2\gamma_1^2|\langle 1_e|\ell_e\rangle|^2[V \pm \omega_c\sqrt{\lambda(X)}]}{\mathcal{N}_0^2\mathcal{N}_e^2\lambda(X)[1+\lambda(X)]\left[\omega_c^2 \mp 2V\omega_c\sqrt{\lambda(X)}\right]}\,, \tag{36}$$

$$\varepsilon^e_2(X) \approx -\frac{V}{2} + \frac{2\gamma_1^2 V|\langle 0'_e|0\rangle|^2}{(\mathcal{N}'_e)^2\omega_c^2\lambda_1^2(X)}\,. \tag{37}$$

The band $\varepsilon^e_2(X)$ exhibits the same behavior as $\varepsilon_2(X)$ obtained in Sec. III A [see Eq. (16)], which arises in both cases from the dominant boundary condition on the component $\tilde{B}$. This corresponds to a moderate holelike dispersion, which interpolates between the bulk energy ε_2 and $-V/2$ as X is pushed farther and beyond the edge. From Eq. (36), the lower branch $\varepsilon^e_{1,-}(X)$ is also holelike and disperses more steeply. As a result, $\varepsilon^e_2(X)$ and $\varepsilon^e_{1,-}(X)$ tend to cross at X satisfying $\varepsilon^e_2(X) = \varepsilon^e_{1,-}(X)$. As in the case discussed in Sec. III B, this crossing is avoided and a gap is opening, given (to leading order in γ_1) by

$$\Delta_e(X) \approx -\frac{\gamma_1}{\sqrt{\lambda(X)}\mathcal{N}_0}|\langle 0|\ell_e\rangle|\,. \tag{38}$$

The resulting edge spectrum is characterized by two separate holelike bands: one interpolating between the bulk state $\varepsilon_1 = V/2$ and a saturated value $-V/2$, and one starting at

ε_2 and steeply dispersing downward without bound. On top of these, the branch $\varepsilon^e_{1,+}(X)$ is largely particlelike and steeply disperses upward for X near or beyond the edge. This behavior is consistent with Fig. 5. It should be noted that the above analysis, based on a perturbative expansion in γ_1, appears to be qualitatively valid even if γ_1 is not small. As we have argued in Secs. III A and III B, the perturbative expansion in fact becomes increasingly more justified as X is pushed farther over the edge.

IV. CONCLUSION

In this paper we have studied edge states of bilayer graphene systems in the quantum Hall regime. Our results show that a variety of edge-state energy structures are possible depending on precise boundary conditions. In some cases, we found that for a continuum model, edge states can disperse from a bulk energy value $\pm V/2$ to $\mp V/2$, while in other cases they may disperse to $\pm\infty$. In yet other cases the edge states may not disperse at all. All these behaviors could be understood qualitatively within the framework of perturbation theory, and in the first of these cases a variational approach allows us to relate the edge-state dispersion to the problem of edge states in single-layer graphene and to the edge dispersion of conventional quantum Hall states.

The complicated dispersions discussed in this paper yield a variety of possible crossings and anticrossings, particularly when spin is included as a degree of freedom and the effects of Zeeman coupling are considered. This rich set of possible spectra for the edge states of bilayer graphene in a magnetic field suggest a variety of possibilities for physical phenomena at the edge, including counterpropagating edge states, spin-filtering,[21] and multicomponent Luttinger liquids. These possibilities will be explored in future research. We note that the phenomenology associated with the predicted edge-state structure is likely to be observable in relatively clean bilayer nanoribbon flakes with straight edges: local impurities and rough edges are expected to localize the edge channels,[36] yielding an insulating state close to zero doping.

ACKNOWLEDGMENTS

We acknowledge useful discussions with R. Moessner, V. G. Pai, and C.-W. Huang. The authors acknowledge the hospitality of KITP-UCSB where this work was initiated, and the Aspen Center for Physics. This work has been financially supported by the US–Israel Binational Science Foundation (BSF) through Grant No. 2008256, the Israel Science Foundation (ISF) Grant No. 599/10, and the NSF through Grant No. DMR1005035.

[1] R. E. Prange and S. M. Girvin, *The Quantum Hall Effect* (Springer-Verlag, New York, 1987).
[2] D. Yoshioka, *The Quantum Hall Effect* (Springer-Verlag, New York, 2002).
[3] S. Das Sarma and A. Pinczuk, *Perspectives in Quantum Hall Effects* (Wiley, New York, 1997).
[4] J. K. Jain, *Composite Fermions* (Cambridge University Press, New York, 2007).
[5] B. I. Halperin, Phys. Rev. B **25**, 2185 (1982).
[6] M. Buttiker, Phys. Rev. B **38**, 9375 (1988).
[7] Z. Hasan and C. L. Kane, Rev. Mod. Phys. **82**, 3045 (2010).
[8] X. L. Qi and S. C. Zhang, e-print arXiv:1008.2026.
[9] I. Zutic, J. Fabian, and S. Das Sarma, Rev. Mod. Phys. **76**, 323 (2004).
[10] A. Fert, Rev. Mod. Phys. **80**, 1517 (2008).
[11] K. S. Novoselov, A. K. Geim, S. V. Mozorov, D. Jiang, Y. Zhang, S. V. Dubonos, I. V. Gregorieva, and A. A. Firsov, Science **306**, 666 (2004).
[12] K. S. Novoselov, D. Jiang, T. Booth, V. Khotkevich, S. M. Morozov, and A. K. Geim, Nature (London) **438**, 197 (2005).
[13] Y. Zhang, Y.-W. Tan, H. L. Stormer, and P. Kim, Nature (London) **438**, 201 (2005).
[14] A. H. Castro Neto, F. Guinea, N. M. R. Peres, K. S. Novoselov, and A. K. Geim, Rev. Mod. Phys. **81**, 109 (2009).
[15] T. Ando, J. Phys. Soc. Jpn. **74**, 777 (2005).
[16] C. L. Kane and E. J. Mele, Phys. Rev. Lett. **95**, 226801 (2005).
[17] D. Huertas-Hernando, F. Guinea, and A. Brataas, Phys. Rev. B **74**, 155426 (2006).
[18] H. Min, J. E. Hill, N. A. Sinitsyn, B. R. Sahu, L. Kleinman, and A. H. MacDonald, Phys. Rev. B **74**, 165310 (2006).
[19] Y. Yao, F. Ye, X.-L. Qi, S.-C. Zhang, and Z. Fang, Phys. Rev. B **75**, 041401 (2007).
[20] L. Brey, Bull. Am. Phys. Soc. **51**, 459 (2006).
[21] D. A. Abanin, P. A. Lee, and L. S. Levitov, Phys. Rev. Lett. **96**, 176803 (2006).
[22] H. A. Fertig and L. Brey, Phys. Rev. Lett. **97**, 116805 (2006).
[23] D. A. Abanin, K. S. Novoselov, U. Zeitler, P. A. Lee, A. K. Geim, and L. S. Levitov, Phys. Rev. Lett. **98**, 196806 (2007).
[24] J. G. Checkelsky, L. Li, and N. P. Ong, Phys. Rev. Lett. **100**, 206801 (2008).
[25] J. G. Checkelsky, L. Li, and N. P. Ong, Phys. Rev. B **79**, 115434 (2009).
[26] Z. Jiang, Y. Zhang, H. L. Stormer, and P. Kim, Phys. Rev. Lett. **99**, 106802 (2007).
[27] E. Shimshoni, H. A. Fertig, and G. V. Pai, Phys. Rev. Lett. **102**, 206408 (2009).
[28] E. McCann and V. I. Fal'ko, Phys. Rev. Lett. **96**, 086805 (2006).
[29] E. V. Castro, K. S. Novoselov, S. V. Morozov, N. M. R. Peres, J. M. B. Lopes dos Santos, J. Nilsson, F. Guinea, A. K. Geim, and A. H. Castro Neto, Phys. Rev. Lett. **99**, 216802 (2007).
[30] We note that within present fabrication techniques, e.g., the chemical vapor deposition (CVD) process, graphene nanoribbons with zigzag edges were found to be more abundant: see Q. Yu *et al.*, Nat. Mater. **10**, 443 (2011).
[31] S. Ryu and Y. Hatsugai, Phys. Rev. Lett. **89**, 077002 (2002).
[32] M. Nakamura, E. V. Castro, and B. Dora, Phys. Rev. Lett. **103**, 266804 (2009).
[33] L. Brey and H. A. Fertig, Phys. Rev. B **73**, 195408 (2006).
[34] G. Granger, J. P. Eisenstein, and J. L. Reno, Phys. Rev. Lett. **102**, 086803 (2009).
[35] H. A. Fertig, Physics **2**, 15 (2009).
[36] H. Xu, T. Heinzel, and I. V. Zozoulenko, Phys. Rev. B **80**, 045308 (2009).